

AD-A090 503

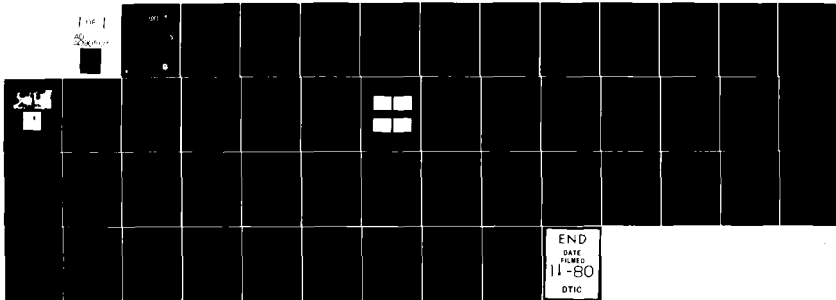
AIR FORCE GEOPHYSICS LAB HANSCOM AFB MA
SWIR STUDIES IN LABCEDE FACILITY: INITIAL FINDINGS.(U)
FEB 80 A R FAIRBAIRN, R GIRNIUS, S J WOLNIK
AFGL-TR-80-0054

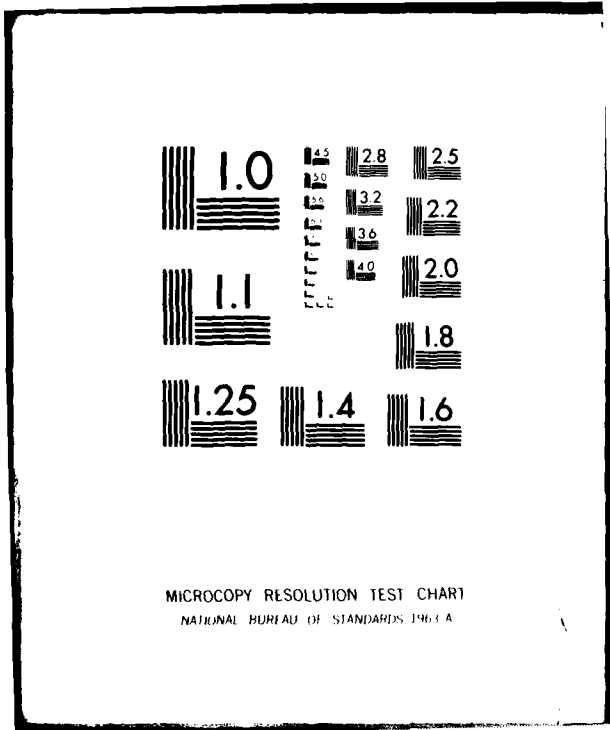
F/G 17/5

UNCLASSIFIED

NL

Fig 1
Scenes





AFGL-TR-68-0854
ENVIRONMENTAL RESEARCH PAPERS, NO. 88

LEVEL



12

B.S.

AD A090503

**SWIR Studies in LABCEDE Facility:
Initial Findings**

A. R. PARBARN
J. GRINUS
S. J. WOLNIK

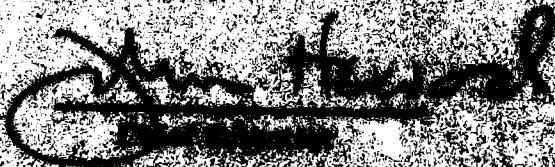
DTIC
EXTRACTED
OCT 16 1980
C

February 1969

This report has been reviewed by the NSD Information Office (OI) and is
releasable to the National Technical Information Service (NTIS).

This technical report has been reviewed and
is approved for publication.

FOR THE COMMANDER

A handwritten signature in dark ink, appearing to read "John H. ...", is written over a horizontal line. The signature is cursive and somewhat stylized.

Environmental research papers

AFGL-ERP-695

Unclassified

SECURITY CLASSIFICATION OF THIS PAGE (When Data Entered)

REPORT DOCUMENTATION PAGE		READ INSTRUCTIONS BEFORE COMPLETING FORM	
1. REPORT NUMBER AFGL-TR-80-0054	2. GOVT ACCESSION NO. AD-A090 503	3. RECIPIENT'S CATALOG NUMBER	
4. TITLE (and Subtitle) SWIR STUDIES IN LABCEDE FACILITY: INITIAL FINDINGS		5. TYPE OF REPORT & PERIOD COVERED Scientific. Interim.	
7. AUTHOR(s) A. R. Fairbairn S. J. Wolnik R. Girnius		6. PERFORMING ORG. REPORT NUMBER ERP No. 695	
9. PERFORMING ORGANIZATION NAME AND ADDRESS Air Force Geophysics Laboratory (OPR) Hanscom AFB Massachusetts 01731		8. CONTRACT OR GRANT NUMBER(s)	
11. CONTROLLING OFFICE NAME AND ADDRESS Air Force Geophysics Laboratory (OPR) Hanscom AFB Massachusetts 01731		10. PROGRAM ELEMENT, PROJECT, TASK AREA & WORK UNIT NUMBERS 61102F 2310G409	
14. MONITORING AGENCY NAME & ADDRESS (if different from Controlling Office) 2310, I25 BARK		12. REPORT DATE 8 February 1980	
16. DISTRIBUTION STATEMENT (of the Report) (17) G4, 7639 Approved for public release; distribution unlimited.		13. NUMBER OF PAGES 49	
17. DISTRIBUTION STATEMENT (of the abstract entered in Block 20, if different from Report)		15. SECURITY CLASS. (of this report) Unclassified	
18. SUPPLEMENTARY NOTES * University of Wisconsin This research was supported by the Defense Nuclear Agency under Subtask I25BHX639. Work Unit No. 02, entitled, "LABCEDE Studies."		15a. DECLASSIFICATION DOWNGRADING SCHEDULE	
19. KEY WORDS (Continue on reverse side if necessary and identify by block number) Short wave infrared radiation Laboratory studies Electron beam excitation Spectroscopic studies Cooled background			
20. ABSTRACT (Continue on reverse side if necessary and identify by block number) An experimental facility has been built to utilize the advantages of cooled optical surfaces in infrared measurements. With liquid nitrogen cryogen, significant enhancement of signal-to-noise ratios in the 1- to 10- micron region and some enhancement at longer wavelengths are obtained. The facility is coupled to an electron-beam generator as the excitation source. At present, data have been obtained in the short-wave infrared radiation (SWIR) in air, nitrogen, and oxygen at pressures in the subtorr region. Oxygen has shown			

DD FORM 1 JAN 75 1473

Unclassified

SECURITY CLASSIFICATION OF THIS PAGE (When Data Entered)

409578

FB

Unclassified

SECURITY CLASSIFICATION OF THIS PAGE(When Data Entered)

20. (Cont)

only atomic line radiation in the 1.6- to 5.6- μ m band. Nitrogen shows substantial radiation in the same wavelength region with frequently overlapping band systems extending to at least 4 μ m, due to several different electronic states. Air shows many of the same systems with NO at 2.7 and 5.4 μ m as the most intense features.

micron

micron

micron

Unclassified

SECURITY CLASSIFICATION OF THIS PAGE(When Data Entered)

Preface

This work has been supported by AFOSR under project 2310. We wish to acknowledge the support of the Defense Nuclear Agency and Major J. Mayo under subtask 125BAHX632.

Accession For	
NTIS GRA&I	<input checked="" type="checkbox"/>
DTIC TAB	<input type="checkbox"/>
Unannounced Justification	<input type="checkbox"/>
By _____	
Distribution/ _____	
Availability Codes	
Dist	Avail and/or Special
A	

Contents

1. INTRODUCTION	7
2. THE LABCEDE EXPERIMENTAL FACILITY	8
2.1 Overview	8
2.2 Electron Beam Parameters	8
2.3 Electron Gun	10
3. INFRARED MEASUREMENTS	13
3.1 Spectrometer Systems	16
3.2 Calibration	16
4. OBSERVATIONS	17
5. NITROGEN	30
5.1 First Positive System ($B^3\Pi_g \rightarrow A^3\Sigma_u$)	31
5.2 Infrared Afterglow ($B'^3\Pi_u \rightarrow B^3\Pi_g$)	34
5.3 The Wu-Benesch Bands ($W^3\Delta_u \rightarrow B^3\Pi_g$)	35
5.4 The McFarlane Bands	36
6. NITRIC OXIDE SPECTRA: VIBRATIONAL TRANSITIONS	39
7. CONCLUSIONS	41
REFERENCES	43
DISTRIBUTION LIST	45

Illustrations

1.	Tank Configuration of LABCEDE	11
2.	Electron Gun Mountings	12
3.	CVF Spectra: 1.6 to 5.6 μm	18
4.	Interferometer Spectra	20
5.	Expanded Wavelength Portions of Figure 4b	21
6.	Equivalent Height in Atmosphere as Function of Pressure and Distance in the LABCEDE Tank	32
7.	Hollow Cathode Source N_2 700 millitorr Pulsed Discharge	38
8a.	N_2 Levels and States	39
8b.	Experimental Potential Curves for N_2 in the Range From 6 to 12 eV	40
8c.	Potential Energy Curves for the $\text{W}^3\Delta_u$ and $\text{B}^3\Pi_g$ States of N_2	40

Tables

1.	Beam Parameters for $E = 5$ kV, 1 mA, 60 cm From Source as a Function of Pressure	10
2.	Infrared Radiation Production Observed With an Instrument With $E = 1$ kV, 1 mA	13
3.	Effect of Background Temperature on D^*	15
4.	Finding List N_2 Infrared Bands	24
4a.	Comparison of Unquenched Strengths of Meinel (M) and 1st Positive (1P) in SWIR Region	28
5.	Relative Excitation Rates for Nitrogen States, Direct From the Ground State	33
6.	Intensities Observed in N_2 First Positive System	34
7.	Intensities in the Wu-Benesch Bands	35
8.	$a^1\Pi \rightarrow a'^1\Sigma$ Band Strengths	36
9.	Intensities (relative) in $w^1\Delta \rightarrow a^1\Pi$ N_2 System	37

SWIR Studies in LABCEDE Facility: Initial Findings

1. INTRODUCTION

Auroral events are usually caused by electron injection into the upper atmosphere. The release of electrons following x-ray absorption gives similar effects after the detonation of nuclear weapons at high altitudes. In both cases, complex chains of physico-chemical reactions occur, leading to infrared radiations which will appear as fluctuations on the normal background. These fluctuations will be observed by satellites of various systems and lead to false identifications unless a capability exists for corrections.

This work has been undertaken for the study of infrared radiation effects in low-pressure air and its constituents, caused by the impact of moderately low energy (less than 10 kV) electrons in a laboratory facility. Although it is not possible to model the upper atmosphere completely in the laboratory, such experiments can be of great value. In particular, although the pressures corresponding to high altitude may be attained, the lack of a long path capability means that signals may be too weak for observation. Accordingly, the experiments are run in apparatus especially designed to enhance the signals. This will be discussed in more detail later.

(Received for publication 7 February 1980)

Within a pressure-path length regime that gives enough emission, a laboratory facility is more flexible and far cheaper than the use of field studies. It offers the advantage of easier and less ambiguous data analysis.

LABCEDE (laboratory cold electron dependent excitation) has been designed and built with emphasis on the application to upper atmospheric problems in the infrared.

2. THE LABCEDE EXPERIMENTAL FACILITY

2.1 Overview

The LABCEDE facility is comprised of a large tank, 4 ft in diam. and 15 ft long, with pumps and viewing ports. Figure 1 gives a schematic arrangement. The inside of the tank has a liner, which is cooled with liquid nitrogen, and purposed to give a low emission infrared background. This enhances the signal-to-noise ratio of the detector viewing the emissions created by the excitation source. The excitation source is an electron beam. Originally, the beam was injected along the axis at EB1 and viewed at P₁ or P₂. Later work has been performed with a beam injected at EB2 and viewed through P₂ or P₄.

2.2 Electron Beam Parameters

While it is simple to model either the pressure or density of the atmosphere under laboratory conditions, it is not possible, in general, to do both simultaneously because of the strong atmospheric gradients. At altitudes below 110 km, the temperature is always below 300°K; it would be possible in LABCEDE to cool the gas appropriately.

With the electron beam presently in use, it has not proved practicable to observe infrared signals at pressures less than 1 millitorr (90 km equivalent altitude, T = 190°K) and while the gas could be cooled to 190°K, it is generally cooled much more for background suppression, a point to be discussed in more detail later. The upper limit of pressure in the experimental chamber is set by the requirement of introducing the electron beam; that is, around 200 millitorr (equivalent altitude 60 km) in this apparatus.

Under the foregoing conditions, the beam parameters may be estimated as follows: The range of primary electron is the distance in which its energy is reduced to the local thermal value. This can be approximated by¹

$$R_p \approx 0.02 E^{7/4} / p \text{ cm} \quad (T = 293^\circ\text{K}) \quad (1)$$

1. Cohn, A., and Caledonia, G. (1970) J. Appl. Phys. 41:3767.

where E is in volts and p in millitorr. On its way to being stopped, the primary electron makes successive collisions which give rise to secondary electrons creating 1 ion-pair, on average, for each 35 V lost. The majority of secondaries created by a beam of the order of 10 kV will have energies up to around 50 V and the range is approximately

$$R_s \approx 100/p \text{ cm} \quad (T = 293^\circ\text{K}) . \quad (2)$$

In most gases, there is a distribution of secondary energies with the scarce high energy electrons (several hundred volts) showing some forward scattering, but for this analysis, it is sufficient to consider the distribution as isotropic.²

The primary electrons, although mainly scattered forward, suffer multiple small angle deflections leading to expansion of the beam. This is given approximately by³

$$r \approx 30(pd)^{1/2} d/E \text{ cm} \quad (T = 77^\circ\text{K}) \quad (3)$$

where r is the radius at which the beam intensity is reduced to $1/e$ of its central value, p the pressure in millitorr, d the beam length in centimeters, and E the accelerating potential in volts. The energy loss of the primary electrons is a function of their energy,¹ but the actual observations made in the LABCEDE facility are early in the beam before much degradation has occurred. For example, the beam is generally run at voltages in excess of 5 kV; at a working pressure of 100 millitorr and room temperature, the range would be 600 cm, but the observations are made at about 60 cm from the beam source. Under these conditions, the energy loss is given by¹

$$\frac{1}{N} \frac{dE}{dx} \approx 10^{-15} \text{ V-cm}^2 \quad (4)$$

where N is the number density of gas molecules, E the energy in volts, and x the path length. These factors have been used to calculate Table 1.

As might be expected, the power density falls with pressure and at the limiting pressure of 1 millitorr, the electrical power deposited in the gas is in the nanowatt per cubic centimeter range. At pressures above 10 millitorr, where primary beam diameter is greater than secondary range, the effect of temperature on power density is not strong.

2. Opal, C. B., Beatty, E. C., and Peterson, W. K. (1972) Atomic Data 4:209.

3. Little, P. F., and Von Engel, A. (1952) Proc. Phys. Soc. 65B:459.

Table 1. Beam Parameters for E = 5 kV, 1 mA, 60 cm From Source as a Function of Pressure. (T = 77°K)

P (millitorr)	Equivalent altitude (km)	Rp (cm)	Rs (cm)	Primary beam diameter (cm)	Power density (W/cm ²)
100	53	150	< 1	56	5×10^{-6}
10	70	1500	3	17.5	1×10^{-6}
1	84	15,000	25	5.6	6×10^{-8}
1(293°K)	92	60,000	100	1	1×10^{-9}

2.3 Electron Gun

Two different guns have been investigated. The first used a three-stage differential pumping system and a Philips⁴ cathode of 1/8-in. diameter. This gun was arranged to fire axially down the 15 ft length of the LABCEDE chamber (Figure 1) using a maximum accelerating potential of 2 kV. It was designed to give a current of 40 mA at 2 kV; in practice the maximum observed was 2 mA. Measurements at various parts of the gun indicated that adequate cathode emission was achieved when the gas pressure in the tank was very low (less than 1 millitorr), but the beam was severely attenuated by the interstage apertures which had to be made small because of a difficulty with the pumping system. A lack of space around the gun required the pumps to be mounted 1 m away and the pumping to be done through long, 2-in. diam, pipes that reduced the pumping speed.* The pumping difficulty resulted in an inability to use experimental pressures greater than 10 millitorr of inert gas. The dispenser cathode proved too sensitive to poisoning, particularly by oxygen and CO₂ as well as air pressures greater than 2 millitorr, reducing the current by a factor of 2. The effect of the terrestrial magnetic field, which caused the beam to hit the side of the tank about 5 ft from EB1, was also troublesome, rendering P₃ and P₄ of no use and the light source was a long way from P₂.

The second beam system⁵ was evolved to improve on the first, making it more useful. The major change was to a directly heated tantalum cathode. This will produce more stray light (because of its higher temperature) than the Philips cathode, but so far it has not been detected against the other stray light in the system. This cathode is not susceptible to poisoning and can be run at higher pressure by at least one order of magnitude. This, in turn, relieves some of the

4. Levi, R. (1955) J. Appl. Phys. 26:639.

* A photograph of the setup is given in Figure 2.

5. The system was based on a commercial welding gun Nuclide Min EB, Nuclide Corp., Acton, Massachusetts.

pumping constraints and the new system uses two diffusion pumps, 6-in. diam each. The apertures between stages were enlarged to about 1-cm diam to minimize beam losses. This allowed working pressures up to 200 millitorr. The accelerating potential was generally run at 5 to 8 kV and currents up to about 10 mA were achieved.

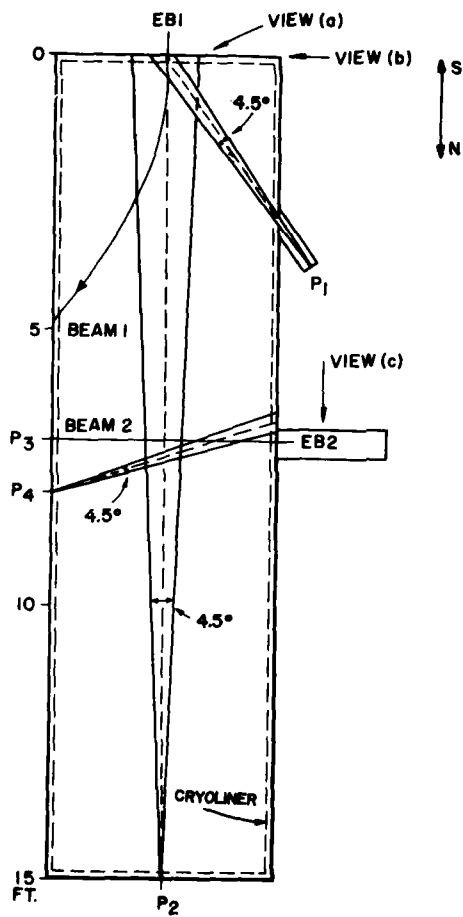
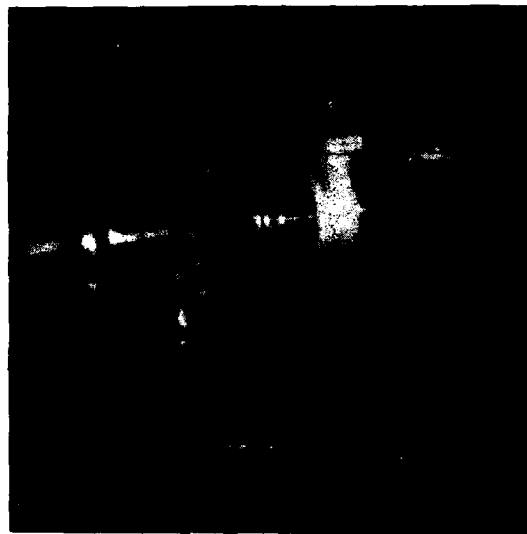


Figure 1. Tank Configuration of LABCEDE (roughly to scale). The fields of view from the various ports and the beam positions are indicated. The arrows labeled view (a), (b), and (c) refer to Figure 2



a

b



c

Figure 2. Electron Gun Mountings. (a) Looking towards EB1, view (a) Figure 1, one observes the cathode towards the RHS of the picture (with the wires hanging down). The pumping lines for the three stages extend towards the lower LHS; (b) looking towards EB1, in view (b) Figure 1. The direction of the beam is towards the left. The pipes for pumping are seen more clearly; (c) The gun at EB2, from view (c) Figure 1. The two stages are connected directly to 6-in. pumps and are interconnected by a gate valve. The cathode insulator may be seen at the LHS. The beam fires towards the right. One of the steering coils is visible on the RHS. The scale in (a), (b), and (c) is given by the 1-ft ruler

Beam currents were monitored with a pick-up coil (Pearson). * This responds only to modulated beams, with a low frequency response down to 30 cps. Consequently, pulses longer than a few milliseconds gave a drooping output. Power supply meters gave measurements of the average current leaving the cathode, but losses in the apertures were such that the correlation between these and the pick-up coil was not good, by a factor of about 2. The lack of correspondence was also a function of gas pressure.

The beam itself was focused by a magnetic coil and steered by means of movable permanent magnets and auxiliary fields due to variable dc currents through Helmholtz-type coils.

3. INFRARED MEASUREMENTS

The major interest in this work is the region from 1 to 5 μm . The room temperature black-body function peaks at 10 μm and at 5 μm is approximately $10^{-3} \text{ W/cm}^2/\mu\text{m}$. An instrument with entrance area A and solid angle of view ω will receive approximately $A\omega \times 3 \times 10^{-4} \text{ W}/\mu\text{m}$ of radiation at 5 μm . If ω is chosen, so that the source fills the optics, the radiation received will be $R A \omega P \eta / (4\pi)$ where P is the power density per cubic centimeter from Table 1 and η is the efficiency of infrared production, and R the beam thickness. This will most likely be a function of pressure itself. If we assume the radiation to be confined in a 10- μm bandwidth, the average radiation received will be $R A \omega P \eta / (40\pi) \text{ W}/\mu\text{m}$.

Table 2. Infrared Radiation Production Observed
With an Instrument With $E = 5 \text{ kV}$, 1 mA .
($T = 77^\circ\text{K}$)

Pressure (millitorr)	RP (W/cm^2)	RP/40 π ₂ ($\text{W}/\mu\text{m}\text{-cm}^2\text{-sr}$)
100	2.9×10^{-4}	2.3×10^{-6}
10	2.4×10^{-5}	1.9×10^{-7}
1	3.3×10^{-6}	2.6×10^{-9}
1 (293°K)	2.0×10^{-7}	1.6×10^{-9}

Most of the energy deposited in the gas will go into ionization and heating. If an estimate of 10 percent is made for infrared production ($\eta = 0.1$), then it is seen from Table 2 that expected power levels of infrared radiation range from 10^{-3} to 10^{-6} of a 300°K black-body background.

* Pearson Electronics Inc., 4007 Transport St., Palo Alto, California.

Alternating current techniques can be used to distinguish small varying signals from strong invariant backgrounds. In the final analysis, these signals use some form of time integration. Drifting of experimental parameters such as pressure, beam current, and so on, can cause difficulties. Photodetectors are generally limited in the signal-to-noise ratio by the background photon flux; and substantial improvements are possible by reducing this background.

In the infrared, this is achieved by cooling the background—blocking off the ambient visible light is quite ineffective. Moreover, all optical components which could possibly radiate to the detector must also be cooled. This relationship between signal-to-noise ratio and input power is given by

$$\frac{S}{N} = \frac{D^* P_s}{\sqrt{A \Delta f}} \quad (5)$$

where P_s is the signal power, A the detector area, and Δf the electrical bandwidth of the circuit in which the measurement is made. A typical requirement in these experiments would be a time resolution of a millisecond and practical detectors may be a few millimeters in size, thus, $(A \Delta f)^{1/2} \approx 10$; thus for $D^* = 10^{10}$, a S/N ratio of unity will be achieved with an incident power of 1 nW. Acceptable spectral resolution requires of the order of 10^{-2} μm bandwidth: From Table 2, the possible powers of radiation range from between 10^{-9} and 10^{-12} W, thus S/N ranging from 1 to 10^{-3} are expected if $D^* = 10^{10}$, which is a typical order of magnitude for a 5- μm detector under 300°K background limited condition, although the very best detectors show $D^* \approx 10^{11}$.

In the background limited case $D^* \propto (Q_b)^{-1/2}$ where Q_b is the background photon flux falling on the detector in its active spectral region. Thus, the S/N ratio of a given measurement can be improved by reducing Q_b . The level of improvement possible is indicated in Table 3, in which a perfect quantum detector is assumed. The wavelength λ_c is the long wave cutoff.

The lowest temperature which may be reached with ease is that of liquid nitrogen, 77°K. As the table indicates, improvements of several orders of magnitude are possible up to 10- μm wavelength. The last column gives values of Noise Equivalent Power (NEP) which have been observed. Although it might appear that D^* can be improved more or less indefinitely as the background temperature is reduced, in practice the resistance of the detector also increases, insulation becomes a problem, and amplifier input impedances cannot be made high enough to avoid loading the detector. A second limitation occurs due to inherent stray capacitance which leads to over-long RC time constants. The references cited in Table 3 show that the current practical limit of NEP is of the order of 10^{-15} watts. Because of a design requirement for the CVF system not to saturate with 300°K backgrounds, the NEP was degraded in this work to 10^{-12} watts.

Table 3. Effect of Background Temperature on D*

λ_c (micrometers)	D*			Noise Equivalent Power (watts) Observed at T _B	
	10 ¹⁰	10 ¹¹	10 ¹⁴		
5	550°K	300°K	130°K	10 ⁻¹⁵ ⁶	77°K
10	500°K	280°K	70°K	10 ⁻¹⁵ ⁷	50°K
20	590°K	250°K	50°K	10 ⁻¹⁵ ^{8,9}	20°K

As already indicated, the entire tank has a cryoliner cooled by liquid nitrogen. This consists of a main shroud which runs the length of the tank as an open-ended cylinder with cutouts for side ports. The shrouding material is finned aluminum plate, connected to each other by tongue and groove. The plates are roughly 1/8-in. thick, 3-in. wide with 20 fins each 3/4-in. high and running the length of the tank. The main cooling pipes run longitudinally, one at the top and the other at the bottom of the shroud. Circumferential pipes at 10-in. intervals connect the upper and lower leads. The shroud plates are welded to these circular pipes. The over-all diameter of the shroud is 1 meter. The ends of the tank and side points are cooled by separate but similar systems. Large chevron baffles are placed over the pumping ports.

It was found that the background levels were rather high unless the ends were blackened with 3M Nextel paint. Further reductions have been made by various measures including further baffling of the chevron baffles (at the expense of some pumping speed) and the taping-up of various joints between ports with aluminum tape. The system took approximately 4 hr to approach equilibrium.

6. Hall, D. N. B., Aiken, R. S., and McCurrin, T. W. (1975) Appl. Opt. 14:450.
7. Keyes, R. J., and Quist, T. M. (1970) Semi Conductors and Semi Metals, Vol. 5, R. K. Willardson and A. C. Beer, Ed., Academic Press, N. Y., p 321.
8. Wyatt, C. L. (1975) Appl. Opt. 14:3086.
9. Dereniak, E. L., Joyce, R. R., and Capps, R. W. (1977) Rev. Sci. Inst. 48:392.

3.1 Spectrometer Systems

Many of the observations have been made with a CVF spectrometer (Utah State University, NS4). The detector is indium antimonide and the CVF is responsive from 1.6 to 5.5 μm . The entire optical system is cooled with liquid nitrogen. As used in this work, the system was not set up for maximum D^* in order that a 300°K black-body could be observed. Thus, the tank itself, prior to cooling could be used as a rough calibration reference.

The filter wheel had a wavelength resolution of about 3 percent and revolved 2 times per second. The Noise Equivalent Spectral Response (NESR) at 5 μm was $3 \times 10^{-9} \text{ W/cm}^2/\text{st}/\mu\text{m}$. The electrical bandwidth was about 200 Hz and the D^* was accordingly about 10^{12} .

This spectrometer was always used at P_2 . It had a field of view of 5 degrees and thus observed about 6 in. of the central part of the beam coming from EB1.

The residual background observed in this work (with the tank cooled) was about 10^{-4} times less than that of the 300°K black-body at 5 μm ; this residual radiation may be observed in some of the results presented. The theoretical intensity ratio between temperatures of 300°K and 77°K is about 10^{12} at 5 μm , which far exceeds the dynamic range possible. This residual radiation must be due to a small leak of radiation at some temperature between 77° and 300°K. Attempts to fit the profile to a temperature were not successful, indicating that several sources may be involved. Since the radiation was not a limiting factor, its suppression was not pursued further.

At gas pressures around 100 millitorr, it is expected (Table 2) that sufficient radiation will be available for observation by a room-temperature limited Michelson interferometer and some measurements made with an instrument having a 6 degree angle of view and a 1-in. entrance aperture. With use of a liquid nitrogen cooled PbS detector, weak signals were observed using P_2 . Much stronger signals were observed at P_4 with the field of view intercepting the radiating region obliquely. The geometry is ill-defined but for identification and survey purposes, this is not important. A typical run with the interferometer took an hour or so, whereas the CVF system took only 0.5 second. The PbS detector has a response to 3.9 μm . Longer wavelengths were observed with the PbSe but with diminished sensitivity over the whole spectral range. We were not able to observe radiation of less than 3- μm wavelengths using the PbSe detector.

3.2 Calibration

For these experiments, the CVF system was not calibrated for intensity. However, the intensity of the room temperature tank gave a rough indication, together with the known gain of the amplifiers. This agreed quite well with an earlier

calibration¹⁰ for a rocket experiment. Due to replacement of parts of the drive train of the CVF wheel, the wavelength calibration made concurrently was lost; the wavelength and features noted were bootstrapped by recognition of certain features which then were fitted with the wheel's known characteristics.

The interferometer used a He-Ne laser as its reference wavelength; it was calibrated by a black-body source run at known temperatures. This was mainly useful for relative measurements because the black-body calibration source was smaller than the field of view which is not uniform over the acceptance angle.

4. OBSERVATIONS

The gases investigated in this work have been air, nitrogen, and oxygen. The excitation conditions differed according to whether the interferometer or CVF spectrometer was used. The former was employed in an ac coupled mode which required pulsing of the beam source. The output signal was digitized at every full wavelength change of the reference fringe system. The slowest rate at which this could be reliably done, and still maintain a fairly steady drive, was once every 2 sec or so. This slow rate was needed to minimize the effects of long lived beam-produced species. Since time scales of the order of 50 msec could be easily envisioned, this gave a repetition rate of about 20 Hz and, thus, the possibility of averaging about 10 samples per point. The length of the pulse was limited by the electronics employed to a maximum of 200 msec. The pulse shape itself was approximately trapezoidal, larger at the front, and a few milliamperes in current. The excitation for the CVF, a direct coupled instrument, was a dc beam of a few milliamperes. In both cases, typical accelerating potentials were 8 kV.

A continuous gas flow was maintained during the experiments but the flow rates tended to be low. At pressures around 100 millitorr the measured pumping speed was 300 cubic feet per minute. With the shroud diameter of 1 m, this gives a gas velocity of around 20 ft/min. With the pulsing rate used this means that some buildup of beam-created permanent species will occur.

Figures 3 through 5 give spectra obtained in these experiments. The nitrogen bands have been identified from a finding list given in Table 4. This has been compiled from several sources; where Frank-Condon factors are available, only bands with a value greater than 0.1 have been included. The list is not exhaustive; that is, it does not include all possible bands.

10. Condon, T., AFGL, Private communication.

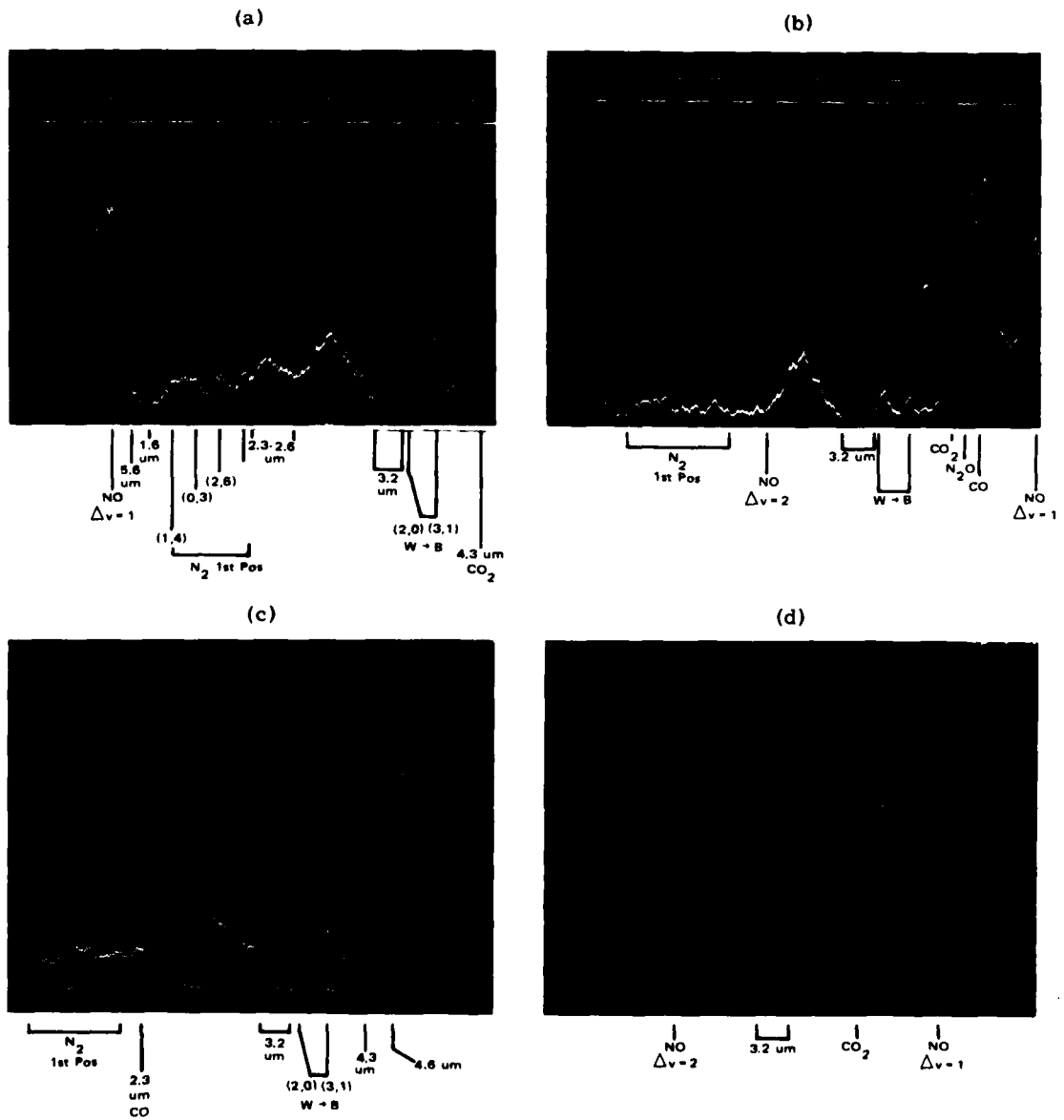


Figure 3. CVF Spectra: 1.6 to 5.6 μ m

◆ Figure 3. CVF Spectra: 1.6 - 5.6 μm

The filter wheel rotates continuously and a "snap shot" scanning one revolution, 1/2 sec, is taken on an oscilloscope. The start time of the sweep is unsynchronized hence the wavelength, which increases from left to right, is displayed at different positions from shot to shot. The two segments comprising the wheel cover 1.6 to 3.2 and 2.8 to 5.6 μm . To avoid confusion (the part of the spectrum between 2.8 and 3.2 μm appearing twice) has been blacked out and the 3.2 μm wavelength has been marked twice. The first half of the wheel has twice the dispersion of the second half. All spectra were obtained with a dc electron beam. Circa 7 kV, 10 mA, and the output displayed is dc so that the stationary background also shows up.

- (a) N_2 gas. $P = 110$ millitorr. The gas had flowed for awhile to improve purity. In terms of wavelength, the first features are N_2 1st positive bands which are indicated. These are followed by emission due to CO starting at 2.3 μm and by NO starting beyond 2.6 μm . After the 3.2 μm point, the two strong features are the Wu-Benesch bands, followed by CO_2 at 4.3 μm which has gone off scale. The next feature, also off scale, is N_2O . The wavelength scan folds back and continues at the left-hand side of the trace, with an off scale feature, probably CO and part of the NO fundamental appearing at 5.4 μm . The drop-off to 5.6 μm is due to detector response and the wavelength scan then repeats. The NO observed must be due to impurity amounts of oxygen since no oxygen was intentionally added.
- (b) The conditions for this run were similar to those for run (a) but the beam had been run for 2 min before the spectrum was taken. The N_2 features, both 1st positive and Wu-Benesch bands, are comparable but the spectrum elsewhere has become totally dominated by CO and CO_2 . There are two traces shown with a scale factor ratio of 40, and the upper trace in (b) has a factor of 0.4 of the trace shown in (a).
- (c) Effect of additions of 3 percent oxygen. The conditions are comparable with the run shown in (a). Scale factors are the same. The N_2 1st positive and W \rightarrow B bands are slightly quenched; N_2O and CO are also diminished. The NO intensity is roughly the same as in (a) where none was added.
- (d) Air, pressure = 8 millitorr. The scale factor is the same as for (c) and (a). The upper trace shows the background, with no electron beam. The beam produces NO and a small amount of CO_2 . Any N_2 features are too weak to be seen. To obtain the true gas spectrum, the background level should be subtracted.

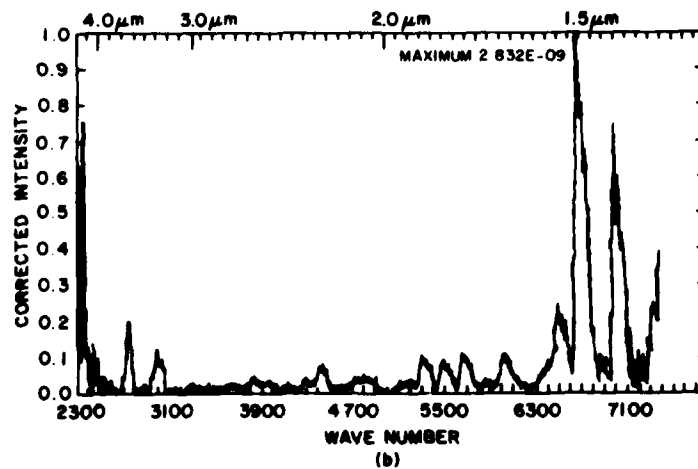
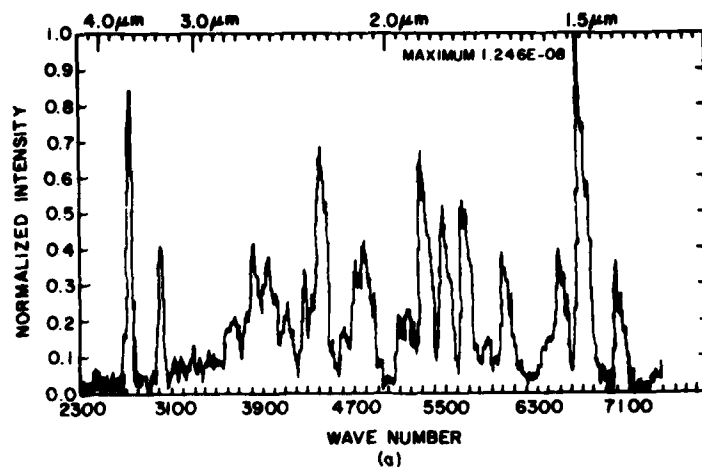


Figure 4. Interferometer Spectra. N₂, p = 120 millitorr.
 (a) Direct output. (b) Intensity after correction by
 black-body measurement

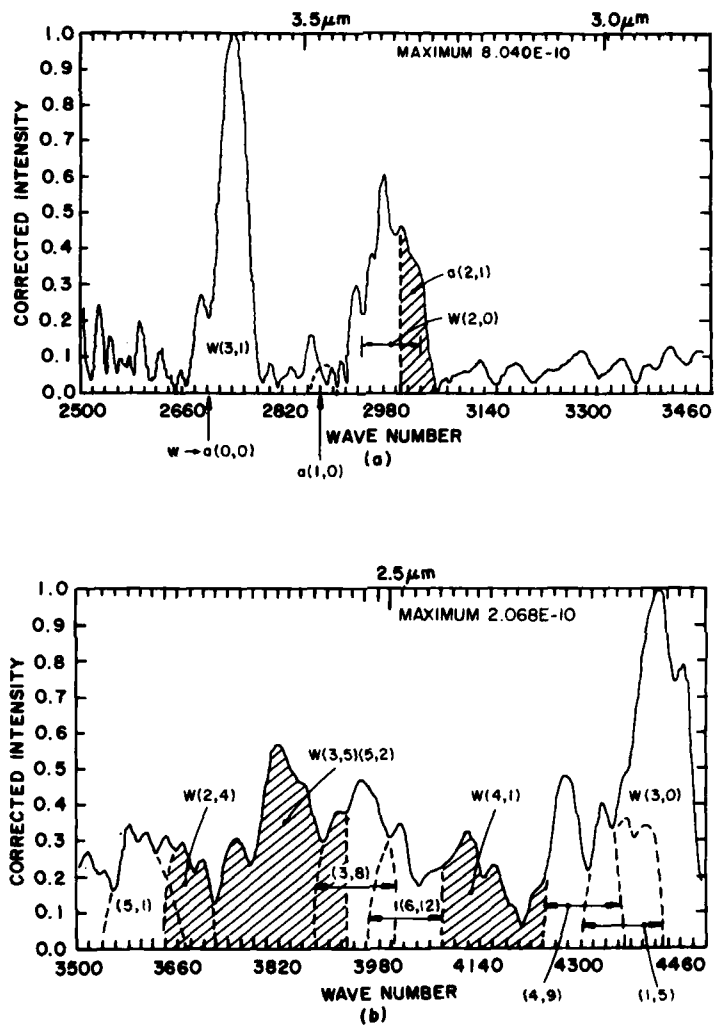


Figure 5. Expanded Wavelength Portions of Figure 4b. The intensities in each of these are normalized to unity for the most intense features. Most of the features have been labeled, using the notation in Table 4, where no prefix is given; for example, (5, 1) the band is identified as N₂ first positive. Where bands overlap, the rough shape has been drawn in, although not necessarily the intensity. Bands mentioned in text and tables, which might occur but cannot be verified, have been indicated in their expected position by arrows

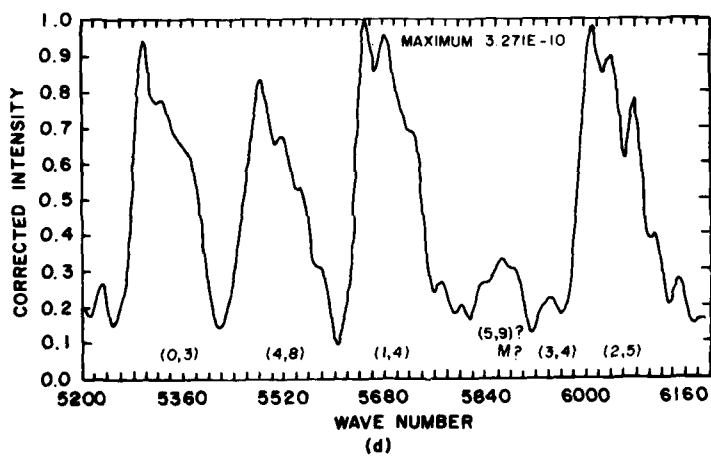
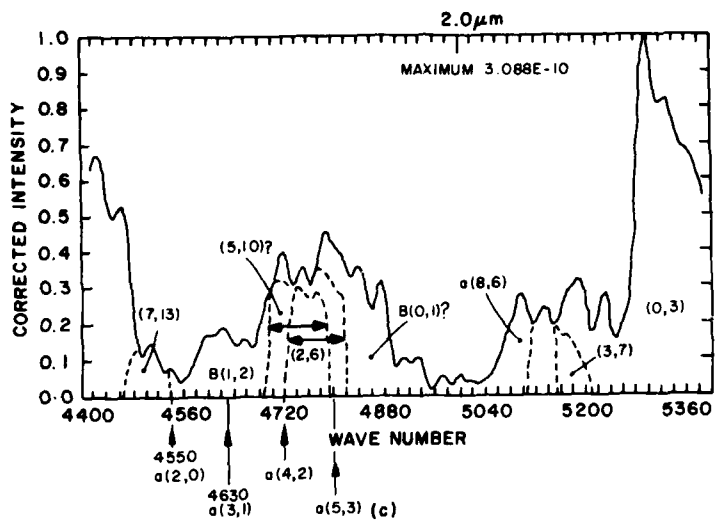


Figure 5. (Cont)

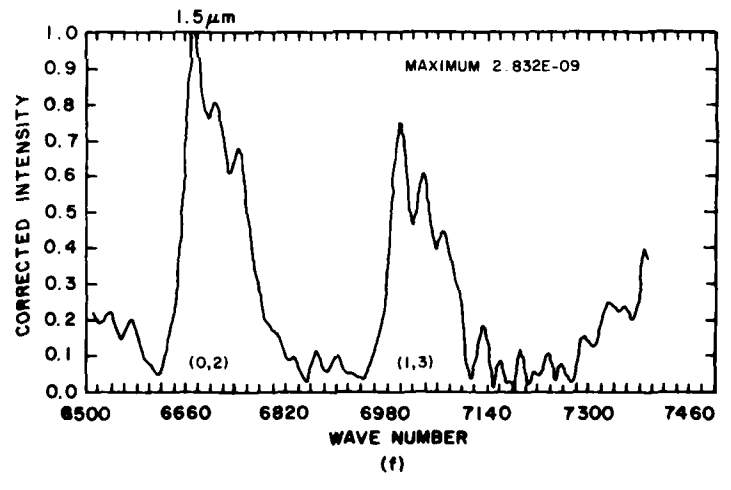
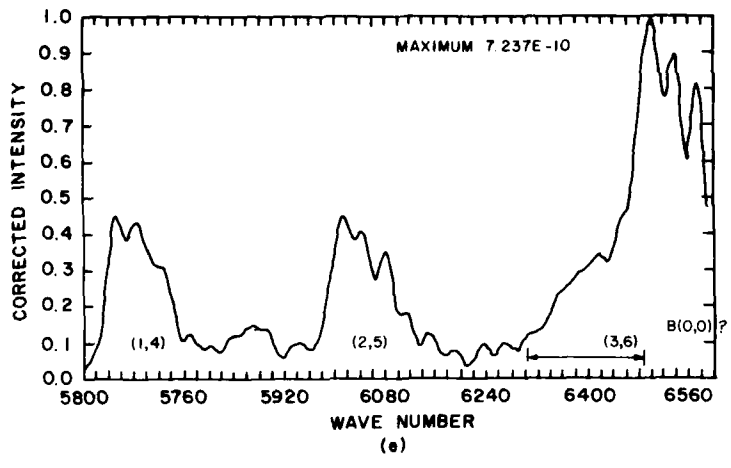


Figure 5. (Cont)

Table 4. Finding List N₂ Infrared Bands

λ (μm)	IP	B	W	w	a
1.05	(0, 0)	(2, 0)			
1.08	(6, 11)	(3, 0)			
1.11		(4, 2)			
1.14		(5, 3)			
1.19	(1, 2)				
1.23	(0, 1)				
1.24		(1, 0)			
1.28		(2, 1)			
1.36	(2, 4)				
1.42	(1, 3)				
1.45				(5, 2)	
1.48	(4, 7)				
1.49	(0, 2)			(6, 3)	
1.53		(0, 0)			(9, 6)
1.55					(8, 5)
1.56	(3, 6)				(7, 4)
1.58		(1, 1)			(6, 3)
1.63		(2, 2)			
1.65	(2, 5)				
1.70	(5, 9)				
1.73				(2, 0)	
1.74			(6, 9)		
1.75		(4, 4)			
1.76	(1, 4)				
1.77			(5, 8)		
1.78				(3, 1)	
1.81	(4, 8)	(5, 5)			
1.83			(4, 7)		
1.84				(4, 4)	
1.87	(0, 3)	(6, 6)	(3, 6)		
1.90				(5, 3)	(8, 14)
1.91			(2, 5)		
1.94					(9, 7)
1.95	(3, 7)				
1.96				(6, 4)	

Table 4. Finding List N₂ Infrared Bands (Cont)

λ (μm)	IP	B	W	w	a
1.97					(8, 6)
2.00					(7, 5)
2.04					(6, 4)
2.07		(0, 1)			
2.08			(7, 3)		(5, 3)
2.09					(5, 10)
2.10	(2, 6)				
2.12	(5, 10)				(4, 2)
2.15		(1, 2)			
2.16					(3, 1)
2.21					(2, 0) (6, 11)
2.23		(2, 3)			
2.24	(7, 13)		(8, 4)		
2.25			(7, 9) (3, 0)*		
2.29	(1, 5)				
2.32	(4, 9)				
2.34				(1, 0)	(7, 12)
2.35			(6, 8)		
2.42				(2, 1)	
2.43			(4, 1)		
2.44			(5, 7) (9, 5)		
2.48					(8, 13)
2.49	(6, 12)				
2.51				(3, 2)	
2.53			(4, 6)		
2.57	(3, 8)				
2.61			(5, 2)	(4, 3)	
2.63					(9, 14)
2.64			(3, 5)		
2.70					(4, 8)
2.71				(5, 4)	
2.75			(2, 4)		
2.80	(5, 11)				

Table 4. Finding List N₂ Infrared Bands (Cont)

λ (μm)	IP	B	W	w	a
2.81			(6, 3)		
2.86					(6, 5)
2.87	(2, 7)				
2.88			(1, 3)		
2.89					(5, 9)
2.96					(5, 4)
3.02			(0, 2)		
3.06					(4, 3)
3.09					(6, 10)
3.14			(7, 4)		
3.16		(0, 2)			
3.19	(4, 10)				(3, 2)
3.32		(1, 3)			(2, 1)
3.33			(2, 0)		
3.42	(6, 13)				
3.47					(1, 0)
3.49			(8, 5)		
3.50		(2, 4)			
3.58					(8, 12)
3.64				(0, 0)	
3.66			(3, 1)		
3.68		(3, 5)			
3.82				(1, 1)	
3.87			(5, 6)		(9, 13)
3.88		(4, 6)			
3.90					(3, 6)
3.91			(9, 6)		
4.01					(9, 9)
4.02				(2, 2)	
4.06			(4, 2)		
4.08	(5, 12)				
4.09		(5, 7)			
4.17				(6, 8)	
4.19			(4, 5)		
4.22				(5, 7)	(8, 8)
4.27					(4, 7)

Table 4. Finding List N₂ Infrared Bands (Cont)

λ (μm)	IP	B	W	w	a
4.46					(7, 7)
4.53			(3, 4)		
4.60			(5, 3)		
4.68					(5, 8)
4.74					(6, 6)
4.75					
4.92			(2, 3)		
5.08					(5, 5)
5.19					(6, 9)
5.47					(4, 4)
5.79					(7, 10)

* This band is observed but its FC factor is less than 0.1.

The column headings refer to the following systems:

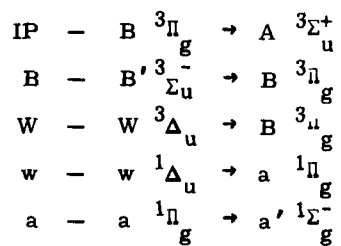


Table 4a. Comparison of Unquenched Strengths of Meinel (M) and 1st Positive (1P) in SWIR Region

λ (μm)	Strength (Relative)	Band	
		M(N_2^+) A \rightarrow X (v' , v'')	IP(N_2) B \rightarrow A (v' , v'')
1.05	3600		(0, 0)
1.11	11,000	(0, 0)	
1.15	980	(1, 1)	
1.23	550	(3, 3)	
1.42	1600		(1, 3)
1.46	2600	(0, 1)	
1.49	440		(0, 2)
1.52	2300	(1, 2)	
1.59	790	(2, 3)	
1.65	880		(2, 5)
1.65	130	(3, 4)	
1.76	490		(1, 4)
1.81	310		(4, 8)
1.87	80		(0, 3)
2.13	150	(0, 2)	
2.24	290	(1, 3)	
2.32	120		(4, 9)
2.36	210	(2, 4)	
2.50	84	(3, 5)	

At the highest target gas pressure used, and to a lesser extent, at the lower pressures, the spectra observed by the CVF system were much stronger in CO, CO₂ than the spectra taken by the interferometer. Some experiments were run with the CVF stopped at the CO₂ peak transmission; it was found that switching off the beam showed a decay whose time constant was of the order of seconds. Being a dc system, the CVF instrument is responsive to such signals, whereas the ac coupled interferometer has a low frequency cutoff of about 1 sec and therefore attenuated long-lived signals. With a PRF of 20 Hz the modulation depth of the CO₂ signal was much smaller than the other signals and not as prominent. The source of the CO₂ is not known of certainty. None was added and the leak rate of the system for air is not enough to explain it. At 77°K, the vapor pressure of CO₂ is less than 10⁻⁷ torr. Thus for any pressure of air greater than 1 millitorr in an equilibrium situation, CO₂ will be preferentially frozen out on the walls. This observation of strong CO₂ signals, and even stronger CO signals, shows that CO₂ is present in unexpectedly large amounts.

The most likely source of this CO₂ is desorption from the walls due to the beam impact. It is well-known that residual gas analyzers attached to vacuum systems show excess CO₂ and CO and also H₂O. In general, conditions on the walls in this system are ill-defined and it is difficult to make even order of magnitude estimates of the amounts of CO₂ to be expected. The energy remaining in the beam (say 1 mA at 10 kV) is sufficient to vaporize 0.01 g of CO₂ on each 200 msec pulse.¹¹ This amount would be more than sufficient to give the observed signals, being equivalent to a gas layer 1 cm thick if the beam hits an area 1 m × 1 m and all its energy is used in dislodging CO₂. During the off-time, most of the CO₂ will be reabsorbed. The observed characteristic time for the CO₂ signal to build up is of the order of 1 sec and a simple one dimensional estimate gives¹²

$$C = C_0 \operatorname{erfc} [x/2 \sqrt{(Dt)}] \quad (6)$$

where C is the concentration at x from a source C₀ after time t has elapsed. Using gas-kinetic estimates for D (500 cm² sec⁻¹ for CO₂ at 77°K and 100 millitorr) and x = 50 cm and t = 1 sec, one finds that the concentration at the center of the tank is 0.1 C₀ where C₀ is some approximate average concentration at the wall. It can hardly be expected that C₀ should be more than 10 percent, leaving a possible maximum of 1 percent at the center of the tank.

The CO observed is almost certainly formed by the dissociative recombination of CO₂⁺ ions; CO is not condensed at 77°K and will remain free until pumped away.

11. Estimates made from data in Handbook of Chemistry and Physics, CRC (1968), p E23.
12. Crank, J. (1956) Mathematics of Diffusion, Oxford University Press, p 19.

At 77°K the vapor pressure of ice is many orders of magnitude less than that of CO₂. It might be expected, however, that water might also be displaced by the beam impact. With the limited spectral resolution available, it is not possible to state whether or not H₂O played any part in the experiment using the CVF. With use of the Michelson interferometer, the OH at 3640 cm⁻¹ was not observed, but such an observation does not warrant the conclusion that H₂O vapor was not present.

The CO₂ and CO impurity problem remains a serious one, for which no adequate solution has yet been found. Catching the electron beam on a brass plate with extra liquid nitrogen cooling coils, thereby minimizing a temperature rise observed on the original shroud, was unsuccessful. Pumping of the chamber to very low pressure before cooling also met with no success. There is no ability at present to "bake out" the surfaces and this observation is not unexpected. Room air contains CO₂ and H₂O in rather indeterminate amounts because of variable humidity and exhaled breath, but it is expected that the H₂O and CO₂ content of this air will be mainly frozen out on the walls, and so the mixture is effectively 21 percent oxygen plus 78 percent nitrogen plus 1 percent argon. Experiments using air from a cylinder, which differs from room air only in H₂O content and perhaps CO₂, did not yield different results. Experiments were also run using a 90 percent nitrogen plus 10 percent oxygen mixture and the results were very similar to those with "air." Strong NO formation was observed with mixtures of nitrogen containing as little as 1 percent O₂, and as Figure 3a shows, it can appear when O₂ is only present in trace amounts.

5. NITROGEN

The ultimate purity level attainable is set by over-all leak rate of the system, together with the pumping speed, after the walls have come to equilibrium. The lowest leak rate observed was a pressure rise of 10 millitorr per hour after closing the pumping valves. The over-all volume of the system is around 10,000 liters so the leak rate (assumed to come from outside and not the shroud) was 30 μm/liters/sec. At a pressure of 100 μm, the pumping speed was about 100 liters per second giving a throughput of 10⁴ μm/liters/sec; thus, the impurity level would be expected to be around 0.3 percent. The throughput decreases at lower pressure until the diffusion pumps can be used. This level of impurity is not considered significant for these survey experiments but it could become a factor if the rigorous exclusion of oxygen is desired.

*"Air" depends on the supplier. Linde calls 21 percent O₂, 79 percent N₂, air; Matheson has some grades which are atmospheric air, compressed, and some grades which are synthetic, that is, contain O₂ plus N₂, but not Ar or CO₂.

Both CVF and interferometer spectra have been obtained in nitrogen. The spectrum was quite weak and the interferometer was used with the PbS detector and, thus, was limited to $4 \mu\text{m}$ wavelengths. The CVF showed the longer wavelengths dominated by CO_2 , CO and residual stray light. No identification of nitrogen features has been made past $4 \mu\text{m}$. The dominant N_2 spectrum observed is the first positive system of nitrogen. Not all bands and features observed can be ascribed to this—in particular, two very strong bands centered at 2760 and 2980 cm^{-1} . Among the first positive bands, some weak features were observed that could not be accounted for in synthetic first positive spectra generated for comparison; the remaining intensities have been ascribed to the B system ($\text{B}' \rightarrow \text{B}$)¹³ and the W system ($\text{W} \rightarrow \text{B}$).¹⁴ The two strong bands already mentioned appear to be W bands.

It is particularly unfortunate that this region of the spectrum was contaminated by the absorption spectrum of a silicone RTV rubber used to mount the detector. The spectra shown have been corrected by the use of a black-body observed under the same conditions. While the correction is valid, it has the effect of adding noise to an already weak and noisy spectrum.

We have thus observed the following states of N_2 : B, W, B. The conditions of the observations were after the beam had traversed about 60 cm of gas at 100 millitorr. Several studies of auroral conditions are appropriate for comparison with this work. Figure 6 has been constructed the equivalent height in the atmosphere as a function of tank path length. Electrons entering the atmosphere traverse a long, very low density path before forming aurorae in the 100-km region. Since the stopping of electrons and degradation of this energy is mainly a function of mass traversed, the figure has been constructed by comparing the integrated mass in a given path length in the tank with the integrated mass between a given altitude and the top of the atmosphere. For example, a particle penetrating to 115 km will traverse the same mass as an electron from the gun which has reached the center of the tank when held at 100 millitorr pressure.

Excitation cross sections for electronic states of molecules tend to have their maximum at threshold, or a few times threshold, and decline with increasing electron energy thereafter. Most states of neutral atoms and molecules fall in the range of a few tens of volts, and it follows that most of the excitation will be performed not by fast primary electrons (a few kiloelectron volts) but by the more numerous and slower ($\sim 50 \text{ eV}$) secondary electrons.

13. Dieke, G. H., and Heath, D. F. (1960) J. Chem. Phys. 33:432.

14. Wu, H. L., and Benesch, W. (1968) Phys. Rev. 172:31.

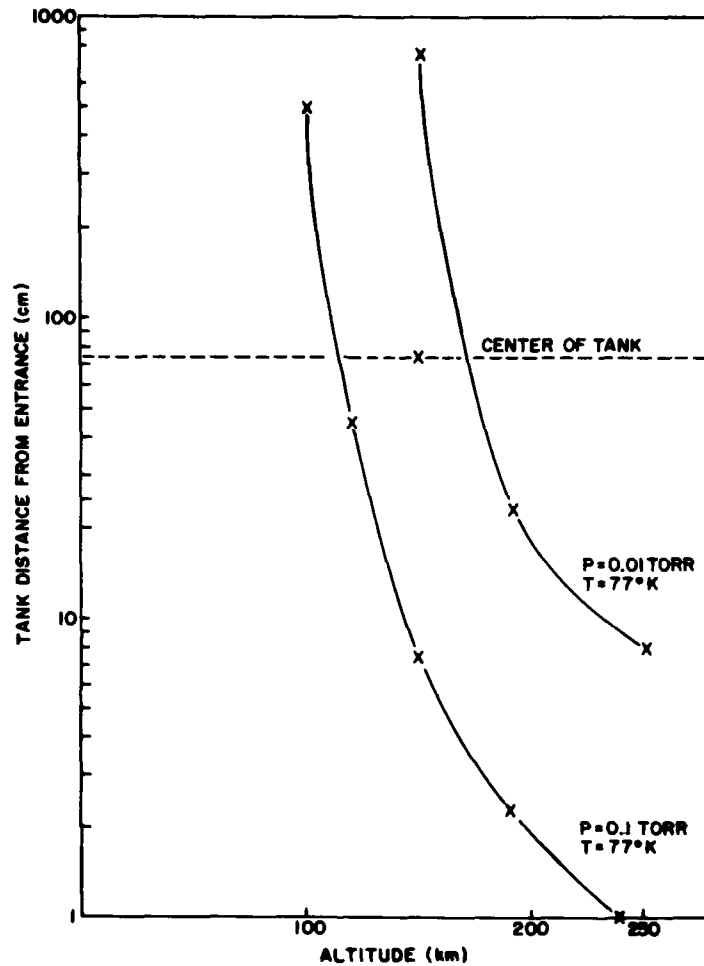


Figure 6. Equivalent Height in Atmosphere as Function of Pressure and Distance in the LABCEDE Tank. The altitude is the depth to which an incoming electron has penetrated

Using this tank-altitude scaling, one finds it of interest to consider the excitation rates to various electronic states. Cartwright¹⁵ has made extensive calculations of auroral excitation and Table 5 has been obtained from his work.

15. Cartwright, D.C. (1978) J. Geophys. Res. 83:517.

Table 5. Relative Excitation Rates for Nitrogen States, Direct From the Ground State. (Assumed 10 keV electron incident on atmosphere. Evaluation made for 110 km altitude)

State	$A^3\Sigma_u$	$B^3\Pi_g$	$W^3\Delta_g$	$B'\Sigma_u$	$a^1\Pi_g$	$w^1\Delta_g$	$C^3\Sigma_u$
Relative Rate	1.0	0.51	0.46	0.23	1.0	0.12	0.46

These rates are dependent on the details of the low energy (20 V) secondary electron spectrum. In our experiments, the low energy secondaries will be most noticeable well away from the center of the beam. The collection optics observed the center part of the beam where the energy has not been so degraded and the effect of secondary electrons will not be noticeable.

Population of a state may be indirect via cascading, as well as direct, and in some cases given by Cartwright, the indirect mechanisms may be dominant, as in the case of the A state. In the conditions run in these experiments, only the C state of nitrogen will not be quenched to any extent and it is expected that around half of the B state will radiate and half be quenched. Other states such as W will be mainly quenched. There is no hard evidence concerning the transition probabilities of the singlet states $w \rightarrow a$, $a \rightarrow a'$ although by assuming their transition moments to be equal to $W \rightarrow B$, and $B \rightarrow A$, respectively, Cartwright, following Freund,¹⁶ has computed their Einstein A coefficients and under our experimental condition both transitions will be appreciably quenched.

Because the spectral resolution in these experiments was not very high ($\approx 20 \text{ cm}^{-1}$), the band identifications are tentative and in what follows we will make some estimates using relative intensities to see how consistent the data are.

5.1 First Positive System ($B^3\Pi_g \rightarrow A^3\Sigma_u$)

Only 6 bands of this system were observed which were fairly free of overlapping or mixing with other bands. These intensities are given in Table 6 and from these are derived relative vibrational populations.¹⁷

The relative intensities (Table 6) given are the same if the peak height is used or the area under the curves.

16. Freund, R. S. (1972) J. Chem. Phys. 56:4344.

17. Einstein A values from D. E. Shemansky and R. L. Broadfoot (1971) J. Quant. Spectros. Radiat. Transfer 11:1385.

Table 6. Intensities Observed in N₂ First Positive System

Band (v', v'')	Relative Intensity	Frequency (cm ⁻¹)	A sec ⁻¹	P _{v'} Relative
(1, 3)	7	7020	1.5 × 10 ⁴	67
(0, 2)	10	6720	1.1 × 10 ⁴	135
(2, 5)	1.2	6030	7.3 × 10 ³	27
(1, 4)	1.2	5670	5.7 × 10 ³	38
(4, 8)	1.1	5500	3.7 × 10 ³	54
(0, 3)	1.1	5320	2.5 × 10 ⁷	82

The first thing to note is the ratio of relative populations of v' = 0 to v' = 1, roughly a factor of 2 in both Δv = -2 and Δv = -3 sequences, but the two sets do not agree. This problem seems to be a weakness of calibration procedure which used a black-body source at about 1200°K. At 1.5 μm its intensity was just sufficient to obtain any signal and so the uncertainty in the reading was high. This becomes less of a problem as the wavelength increases and the Δv = -3 data are considered more reliable. The populations fall from vibrational levels 0 to 2 and then rise to level 4. According to Cartwright, the direct excitation of B state gives increasing population through levels 3 to 4, after which lesser populations are obtained while the glow discharge experiments of Ravodina et al¹⁸ find a continuous decline in B state population with increasing vibrational level, and at low vibrational levels the effect of cascading from the C state was found to be important. Our results fall closer to the category of results observed by Oldman and Broida¹⁹ who found that oxygen atoms could profoundly alter the first positive radiation intensity and its distribution, presumably by producing A state which can then be transferred to B state by collisional perturbation. These matters are not well understood and will be further pursued in later work.

5.2 Infrared Afterglow (B' Π_u - B³ Π_g)

The main part of this system lies in the water infrared below 1 μm. The band at 6520 cm⁻¹ on Figure 5e is probably the (0, 0) band of this system. The rest of the Δv = 0 sequence will be strongly overlapped by first positive bands. The auroral intensity estimates of Cartwright indicate the B' population will be small compared with B when the vibration quantum number is low. The Δv = 1 sequence is located

18. Ravodina, O. V., Popova, T. N., Eliseev, A. A., and Smolyakov, S. S. (1973) Opt. and Spectroscopy 34:243.

19. Oldman, R. J., and Broida, H. P. (1968) J. Chem. Phys. 51:2254.

at 2.07 μm and up but this region is strongly overlapped by possible McFarlane ($a \rightarrow a'$) bands as well as first positive. With our resolution, identification is tentative.

5.3 The Wu-Benesch Bands ($W^3\Delta_u \rightarrow B^3\Pi_g$)

The two outstanding features observed at 2760 and 2980 cm^{-1} have been identified as W bands (3, 1) and (2, 0), respectively, and several other features in the strongly overlapped region between 3500 and 4500 cm^{-1} have also been labeled as belonging to this system. As already mentioned, the bands in the 3000 cm^{-1} region have been affected by an instrumental factor which makes the exact profiles uncertain. Table 7 gives the strength and excitation data for this system.

Table 7. Intensities in the Wu-Benesch Bands

Band (v', v'')	Frequency cm^{-1}	$W^3\Delta \rightarrow B^3\Pi$ Strength sec^{-1}	Excitation Factor $X^1\Sigma(0) \rightarrow W^3\Delta(v')$	$Ef \times Sx\nu$ Relative
(4, 2)	2463	1.2×10^3	0.067	2.0
(3, 1)	2730	1.9×10^3	0.044	2.3
(2, 0)	3000	1.8×10^3	0.023	1.2
(2, 4)	3640	2.4×10^3	0.023	2.0
(3, 5)	3800	2.7×10^3	0.044	4.5
(4, 6)	3950	2.5×10^3	0.067	6.7
(3, 0)	4450	2.3×10^3	0.044	4.5

The excitation factor is the Frank-Condon factor for the transition from the $X^1\Sigma(v=0)$ state of nitrogen (ground state). For electron energies well away from the threshold, this should give a good estimate of relative excitation. The strength of figures are Einstein probabilities from Covey et al.²⁰ The final column is the product of the three preceding ones in arbitrary units.

The main possible overlapping in this region comes from the singlet system (McFarlane bands)²¹ $w \rightarrow a$ and $a \rightarrow a'$. The $W \rightarrow B$ transition probabilities have been given by Covey et al.²⁰ who estimated that with comparable excitation rates the $W \rightarrow B$ system should be comparable in intensity to the $B \rightarrow A$ and with our

20. Covey, R., Saum, K. A., and Benesch, W. (1973) J. Opt. Soc. Am. 63:592.

21. McFarlane, R. A. (1966) J. Quantum Electronics 2:229; also (1965) Phys. Rev. 140A:1070.

identification, this is what is observed. In fact, our intensities indicate that the population of W state should be higher than that of B state, in agreement with Cartwright's auroral estimates.

5.4 The McFarlane Bands ($a^1\Pi \rightarrow a'\Sigma$ and $w^1\Delta \rightarrow a^1\Pi$)

These singlet systems²¹ might be expected to be strong since there is no spin change on excitation from the N_2 ground state, and according to Cartwright's calculations $a \rightarrow a'$ might be comparable with $W \rightarrow B$ and $B \rightarrow A$. In these experiments, the only features observed which could possibly be ascribed to $a \rightarrow a'$ was the (2, 1) band, which falls in the 3000 cm^{-1} region and would either be the feature there, here identified as $W(2, 0)$, or be mixed with it. The lack of strong features in the 3000 to 3500 cm^{-1} region may be taken as evidence against the 3000 cm^{-1} band being the $a \rightarrow a'$ (2, 1) band unless the $v' = 2$ level is preferentially populated. There are some bands in the mixed-up 4700 cm^{-1} region which could be due to $a \rightarrow a'$ and their positions are indicated in Figure 5c. Table 8 has been constructed to give relative intensities in the bands of the $a \rightarrow a'$ system.

Table 8. $a^1\Pi \rightarrow a'^1\Sigma$ Band Strengths

Band (v', v'')	Frequency cm^{-1}	Strength	Excitation Factor $X(0) \rightarrow a(v')$	Total Strength
(1, 0)	2900	35	0.12	4.2
(2, 1)	3000	49	0.17	8.4
(3, 2)	3140	49	0.18	8.8
(4, 3)	3270	39	0.16	6.2
(5, 4)	3400	30	0.12	3.6
(2, 0)	4550	30	0.17	5.1
(3, 1)	4630	74	0.13	13.4
(4, 2)	4720	120	0.16	19.0
(5, 3)	4800	150	0.12	18.0

The band strengths are given as relative values of $\nu^4 q \text{Re}^2(r)$ where ν is the frequency, q the Frank-Condon factor and $\text{Re}(r)$ is taken as the same as for $B \rightarrow A$. The former have been calculated by Benesch et al, and are published in Lofthus and Krupenie.²² The transition moment variation is from Shemansky and Broadfoot.²³

22. Lofthus, A., and Krupenie, P. (1977) J. Phys. & Chem. Ref. Data 6:113.

23. Shemansky, D. E., and Broadfoot, R. L. (1977) J. Quant. Spectros. Radiat. Transfer 11:1385.

Using these intensity estimates, one notes that the (2, 0) band should be comparable in intensity with the (2, 1). Since the observed intensity in the (2, 0) wavelength region lies in the noise, the main part of the observed feature at 3000 cm^{-1} cannot be due to the (2, 1) band of $a \rightarrow a'$.

$w^1\Delta \rightarrow a^1\Pi$

Some relative intensities are given in Table 9, again using the previous assumptions.

Table 9. Intensities (relative) in $w^1\Delta \rightarrow a^1\Pi \text{ N}_2$ System

Band (v', v'')	Frequency cm^{-1}	Strength	Excitation Factor	EF \times S
(0, 0)	2760	74	0.003	0.22
(1, 1)	2620	23	0.014	0.28
(2, 2)	2500	4	0.035	0.14
(1, 0)	4280	186	0.014	2.6
(2, 1)	4150	182	0.035	6.3
(3, 2)	3990	128	0.062	8.0
(2, 0)	5800	174	0.035	6.1
(3, 1)	5600	300	0.062	18
(4, 2)	5420	345	0.087	30

In this case, it is not clear-cut to dismiss the 2760 feature in our spectra as not $w \rightarrow a$. The $\Delta v = 1$ and 2 sequences both fall in very overlapped regions of the spectrum and cannot be compared in the data available.

Both Cartwright (auroral calculations), Table 5, and Freund have estimated that w state population will be considerably less than a $^1\Pi$ state, but Cartwright's estimates of the $w \rightarrow a$ transition probabilities are greater than those of the $a \rightarrow a'$ and so band intensities may be expected to be comparable. If this is so, then since the 3000 cm^{-1} feature is not $a \rightarrow a'$, the 2760 feature is probably not $w \rightarrow a$. A higher spectral resolution is required to distinguish with certainty whether the transition is a singlet or a triplet.

There is a problem with the radiation observed at 3.3 and 3.6 μm which cannot be fully explained at present. It has already been argued that it can hardly be $a \rightarrow a'$, and while $w \rightarrow a$ may make a small contribution, it is mainly $W \rightarrow B$. Both $W \rightarrow B$ and $w \rightarrow a$ have bands at around 4.0 μm , the $W \rightarrow B$ (4, 2) at 2463 cm^{-1} (2, 2) and $w \rightarrow a$ at 2490 cm^{-1} and in Tables 7 and 9 they are estimated as being comparable in intensity with the radiation in the 2750 cm^{-1} region, being roughly 80 percent

of it. The $a \rightarrow a'$ does not have a strong band in the $4 \mu\text{m}$ region. Our interferometer results cannot give information in the $4 \mu\text{m}$ region because of the Pbs cut-off but the CVF is responsive and has shown no significant radiation in the $4\text{-}\mu\text{m}$ region.

Tables 7 and 9 have been constructed assuming the excitation is from $v=0$ in $X^1\Sigma$ (the N_2 ground state) to the upper level of the transition. Our results indicate that either the transition probabilities used are seriously in error, or other mechanisms are involved. We are not able at this time to determine what effects are occurring, but we have observed radiation at $4 \mu\text{m}$ in a different excitation source.* This was a hollow cathode lamp run at a higher pressure (700 millitorr) and much higher current density (A/cm^2 instead of mA/cm^2). A portion of the spectrum obtained (uncorrected for response) is shown in Figure 7. The feature at 2200 cm^{-1} is N_2O impurity but the other features are due to N_2 . For the present, the identification of the 2760 feature as a W band will be retained.

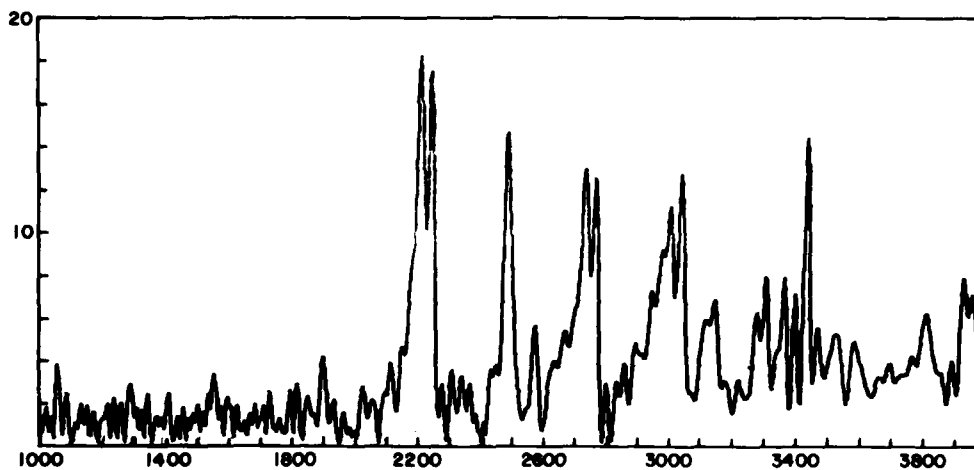
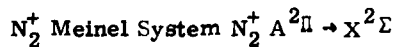


Figure 7. Hollow Cathode Source N_2 700-millitorr Pulsed Discharge



This infrared active system has not been identified in this work. This is not surprising since it is an ionic emitter and is expected to be rapidly quenched, even

* A. R. Fairbairn, Previously unpublished.

at our pressures. Rough estimates indicate that it will not be a major emitter until pressures in the 1-millitorr region are investigated. Relative strengths for the Meinel and first positive system (no quenching) are given in Table 4a.

6. NITRIC OXIDE SPECTRA: VIBRATIONAL TRANSITIONS

The data obtained in both the fundamental region and the overtone, Figure 3, clearly show structure which is attributable to chemiluminescence. High levels of vibration are observed and this is most likely to be due to the reaction $N(^2D) + O_2 \rightarrow NO + O$. The reaction with $N(S)$ cannot be responsible for the observations since it requires an activation energy of about 7 kcal/mole giving a Boltzmann factor of e^{-50} at 77°K. More work is required on this important system and will be addressed in future work.

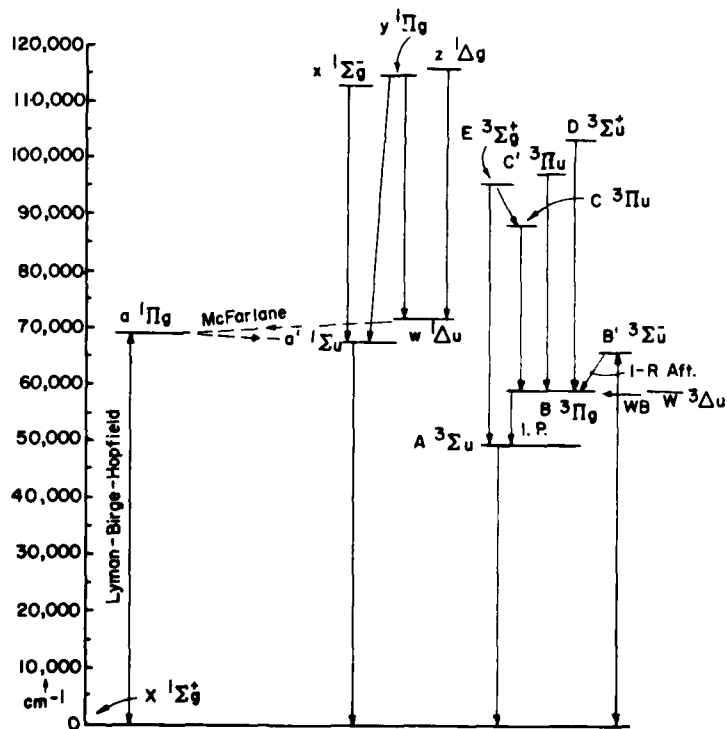


Figure 8a. N₂ Levels and States [From R. A. McFarlane, IEEE J. Quantum Elec. 2:229 (1966)]

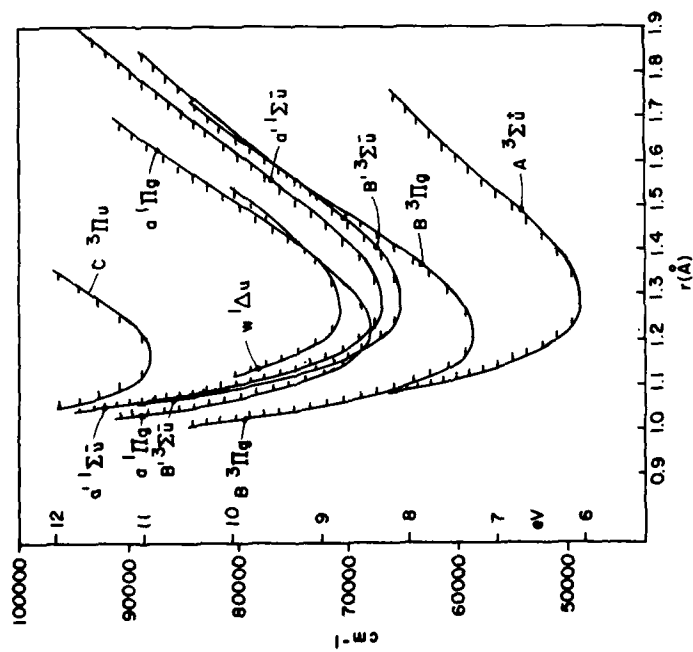


Figure 8b. Experimental Potential Curves for N_2 in the Range From 6 to 12 eV [From Benesch, Vanderslice, Tilford and Wilkinson, *Astrophys. J.* 144:408 (1966)]

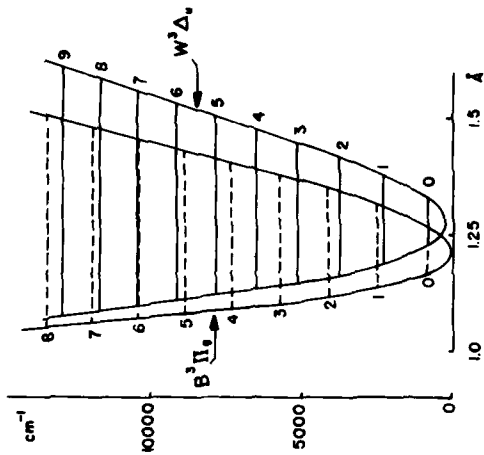


Figure 8c. Potential Energy Curves for the $W^3\Delta_u$ and $B^3\Pi_u$ States of N_2 [From Lofthus and Krupenie, *J. Phys. and Chem. Ref. Data* 6:113 (1977)]

7. CONCLUSIONS

The LABCEDE facility has proved capable of generating detectable infrared radiation in the 1- to 5- μm region in gas pressure as low as 100 millitorr. Chemiluminescence from nitric oxide has been observed at 77°K. Several band systems have been excited in N_2 and the $W \rightarrow B$ system has been found to be of comparable intensity to the $B \rightarrow A$.

References

1. Cohn, A., and Caledonia, G. (1970) J. Appl. Phys. 41:3767.
2. Opal, C.B., Beatty, E.C., and Peterson, W.K. (1972) Atomic Data 4:209.
3. Little, P.F., and Von Engel, A. (1952) Proc. Phys. Soc. 65B:459.
4. Levi, R. (1955) J. Appl. Phys. 26:639.
5. The system was based on a commercial welding gun Nuclide Min EB, Nuclide Corp., Acton, Massachusetts.
6. Hall, D.N.B., Aiken, R.S., and McCurrin, T.W. (1975) Appl. Opt. 14:450.
7. Keyes, R.J., and Quist, T.M. (1970) Semi Conductors and Semi Metals, Vol. 5, R.K. Willardson and A.C. Beer, Ed., Academic Press, N.Y., p 321.
8. Wyatt, C.L. (1975) Appl. Opt. 14:3086.
9. Dereniak, E.L., Joyce, R.R., and Capps, R.W. (1977) Rev. Sci. Inst. 48:392.
10. Condron, T., AFGL, Private communication.
11. Estimates made from data in Handbook of Chemistry and Physics, CRC (1968) p-E23.
12. Crank, J. (1956) Mathematics of Diffusion, Oxford University Press, p 19.
13. Dieke, G.H., and Heath, D.F. (1960) J. Chem. Phys. 33:432.
14. Wu, H.L., and Benesch, W. (1968) Phys. Rev. 172:31.
15. Cartwright, D.C. (1978) J. Geophys. Res. 83:517.
16. Freund, R.S. (1972) J. Chem. Phys. 56:4344.
17. Einstein A values from Shemansky, D.E., and Broadfoot, R.L. (1971) J. Quant. Spectros. Radiat. Transfer 11:1385.
18. Ravodina, O.V., Popova, T.N., Eliseev, A.A., and Smolyakov, S.S. (1973) Opt. and Spectroscopy 34:243.

References

19. Oldman, R. J., and Broida, H. P. (1968) J. Chem. Phys. 51:2254.
20. Covey, R., Saum, K. A., and Benesch, W. (1973) J. Opt. Soc. Am. 63:592.
21. McFarlane, R. A. (1966) J. Quantum Electronics 2:229; also (1965) Phys. Rev. 140A-1070.
22. Lofthus, A., and Krupenie, P. (1977) J. Phys. & Chem. Ref. Data 6:113.
23. Shemansky, D. E., and Broadfoot, R. L. (1971) J. Quant. Spectros. Radiat. Transfer 11:1385.

DISTRIBUTION LIST

DEPARTMENT OF DEFENSE

Director
Defense Advanced Rsch. Proj. Agency
Attn: LTC W.A. Whitaker

Director
Defense Nuclear Agency
Attn: TITL Tech. Library (3 copies)
Attn: TISI Archives
Attn: RAEV Harold C. Fitz, Jr.
Attn: RAAE Lt/Col. McKechney
Attn: RAAE Capt. Peter Luna
Attn: RAAE Dr. Patrick Crowley
Attn: RAAE Maj. R. Bigoni

Dir. of Defense Rsch. & Engineering
Department of Defense
Attn: DD/S&SS (OS) Daniel Brockway

Commander
Field Command
Defense Nuclear Agency
Attn: FCPR

Chief Livermore Division
FLD Command DNA
Attn: FCPRI

DEPARTMENT OF THE ARMY

Commander/Director
Atmospheric Sciences Laboratory
U.S. Army Electronics Command
Attn: DRSEL-BL-SY-A.F. Niles
Attn: H. Ballard

Commander
Harry Diamond Laboratories
Attn: DRXDO-NP, F.H. Wiminetz
(2 Copies)

Superintendent
Naval Post Graduate School
Attn: Rsch Rpts Librarian

Commander
Naval Intelligence Support Center
Attn: Document Control

Director
BMD Advanced Technical Center
Attn: ATC-T, M. Capps
Attn: ATC-O, M. Davies

Dep. Chief of Staff for Rsch. Dev & Accout.
Department of the Army
Attn: MCB Division
Attn: DAMA-CSZ-C
Attn: DAMA-WSZC

Director
U.S. Army Ballistic Rsch. Labs.
Attn: John Mester
Attn: Tech. Library

Commander
U.S. Army Electronics Command
Attn: Inst. for Expl. Research
Attn: Weapons Effects Section

Commander
CORADCOM
Attn: PP-Library
Attn: DRDCO-COM-D

DEPARTMENT OF THE NAVY

Commander
Naval Oceans Systems Center
Attn: Code 2200 William Moler

Director
Naval Research Laboratory
Attn: Code 7712 D.P. McNut
Attn: Code 6701 J.D. Brown
Attn: Code 2600 Tech. Library
Attn: Code 7175J C.Y. Johnson
Attn: Code 6700 T.P. Coffey
Attn: Code 7709 Wahab Ali
Attn: Code 6780 D.F. Strobel
Attn: Code 6780 P. Julienne
Attn: Code 67800 J. Fedder
Attn: Code 6780 S. Ossakow
Attn: Code 6707 J. Davis

Commander
Naval Surface Weapons Center
Attn: Code WA 501 Navv NUC
Programs Office
Attn: Technical Library

DISTRIBUTION LIST (Cont)

DEPARTMENT OF THE AIR FORCE

AF Geophysics Laboratory, AFSC
Attn: LKB, K.S.W. Champion
Attn: OPR, A.T. Stair, Jr.
Attn: OPR, P.G. Doyle
Attn: OPR, R. Murphy
Attn: LKO, R. Huffman
Attn: OPR, J. Kennealy

AF Weapons Laboratory, AFSC
Attn: Maj. Gary Ganong, DES

**Commander
ASD**
Attn: ASD-YH-EX-LTC R. Leverette

SAMSO/AW
Attn: SZJ Lt. Col. Doan

SAMSO/YN
Attn: Maj. P. Sivgals

AFTAC
Attn: Tech Library
Attn: TD

**HQ
Air Force Systems Command**
Attn: DLS
Attn: Tech Library
Attn: DLCAE
Attn: DLTW
Attn: DLXP
Attn: SDR
Attn: RDQ

US ENERGY RSCH. AND DEV. ADMIN

**Division of Military Application
U.S. Energy Rsch. & Dev. Admin.**
Attn: DOC CON

Los Alamos Scientific Laboratory
Attn: DOC CON for H.V. Argo
Attn: DOC CON for M.B. Pongratz
Attn: DOC CON for R. Brownlee
Attn: Group AP-4, MS 567
Attn: DOC CON for J. Zinn

**University of California
Los Alamos Scientific Laboratory**
Attn: Librarian MS 362

Sandia Laboratories
Attn: DOC CON for W.B. Brown,
Org. 1353
Attn: Tech Library Org. 3141

**Argonne National Laboratory
Records Control**
Attn: DOC CON for D.W. Green
Attn: DOC CON for LIR SVCS Rpts
Sec.
Attn: DON CON for G.T. Reedy

**University of California
Lawrence Livermore Laboratory**
Attn: W.H. Duewer, L-262
Attn: J. Chang, L-71

**U.S. Energy Rsch. & Dev. Administration
Division of Headquarters Services,
Library Branch**
Attn: DOC CON for Class. Tech.
Library

OTHER GOVERNMENT

**Department of Transportation
Office of the Secretary**
Attn: S.C. Coroniti

**NASA
Langley Station**
Attn: Tech. Library

DISTRIBUTION LIST (Cont)

NASA
Ames Research Center
Attn: N-245-3 R. Whitten

Department of the Army
Bal. Missl. Def. Adv. Tech. Ctr.
Attn: W.O. Davies

Federal Aviation Administration
Attn: HAFP/AEQ-10/James W. Rogers

Central Intelligence Agency
Attn: ED/SI RM 5G48 HQ Bldg.
Attn: NED/OS I-2G4R HQS

Department of Commerce
National Bureau of Standards
Attn: Sec. Officer for M. Krauss
Attn: Sec. Off. for L.H. Gevantman

National Oceanic & Atmospheric Admin.
Environmental Research Laboratories
Department of Commerce
Attn: G. Reid
Attn: E. Ferguson
Attn: F. Fehsenfeld

DEPARTMENT OF DEFENSE CONTRACTORS

Science Applications, Inc.
Attn: D.G. Hopper

Aero-Chem Research Laboratories, Inc.
Attn: A. Fontign
Attn: H. Pergament

Aerodyne Research, Inc.
Attn: F. Bien
Attn: M. Camac

Aerospace Corporation
Attn: N. Cohen
Attn: H. Mayer
Attn: R.J. McNeal
Attn: T.D. Taylor
Attn: J. Reinheimer
Attn: R.D. Rawcliffe
Attn: R. Herm

Battelle Memorial Institute
Attn: H.L. LaMuth
Attn: STOIAC

Brown Engineering Company, Inc.
Attn: N. Passino

General Research Corporation
Attn: D. Jones
Attn: J. Ise, Jr.

California At Riverside, University of
Attn: J.N. Pitts, Jr.
Attn: A.M. Winer

California At San Diego, University of
Attn: S.C. Lin

California University of Berkley
Attn: Sec. Off. for H. Johnston
Attn: Sec. Officer for Dept of
Chem., H.L. Strauss

Calspan Corporation
Attn: C.E. Treanor
Attn: J.M. Grace
Attn: M.G. Dunn
Attn: W. Wruster

University of Colorado
Astro-Geophysics
Attn: J.B. Pearce

Colorado, University of
Office of Contracts and Grants
Attn: G.M. Lawrence, LASP

Concord Sciences
Attn: E.A. Sutton

University of Denver
Space Science Laboratory
Attn: B. Van Zyl

University of Denver
Denver Research Laboratory
Attn: Sec Officer for D. Murcray

DISTRIBUTION LIST (Cont)

AVCO-Everett Research Laboratory Inc.
Attn: Tech. Library
Attn: C.W. Von Rosenberg, Jr.

General Electric Company
Space Division
Attn: M.H. Bortner, Space Sci. Lab
Attn: J. Burns
Attn: F. Alyea
Attn: P. Zavitsands
Attn: R.H. Edsall
Attn: T. Baurer

Geophysical Institute
University of Alaska
Attn: J.S. Wagner

Lowell University of
Center for Atmospheric Research
Attn: G.T. Best

Lockheed Missiles and Space Company
Attn: J. Kumer, Dept 52-54
Attn: J.B. Cladis, Dept 52-12, B202
Attn: B.M. McCormac, Dept 52-54
Attn: T. James, Dept 52-54
Attn: M. Walt, Dept 52-10
Attn: R.D. Sears, Dept 52-54

Institute for Defense Analysis
Attn: E. Bauer
Attn: H. Wolfhard

Mission Research Corporation
Attn: D. Archer
Attn: D. Fischer
Attn: M. Scheibe
Attn: D. Sappenfield
Attn: D. Sowle

Photometrics, Inc.
Attn: I.L. Kofsky

Berkeley Research Associates
Attn: J.B. Workman

Physical Dynamics, Inc.
Attn: A. Thomas

General Electric Company
Tempo-Center for Advanced Studies
Attn: DASAIC
Attn: W.S. Knapp
Attn: T. Stephens
Attn: D. Chandler
Attn: V.R. Strull

Physics International Company
Attn: DOC CON for Tech Library

Pittsburg, University of the Comwth
System of Higher Education
Attn: W.L. Fite
Attn: M.A. Biondi
Attn: F. Kaufman

R&D Associates
Attn: R. Latter
Attn: R.G. Lindgren
Attn: B. Gabbard
Attn: R. Lelevier
Attn: A.L. Latter
Attn: F. Gilmore
Attn: H.J. Mitchell

Rand Corporation
Attn: C. Crain

Science Applications, Inc.
Attn: D.A. Hamlin
Attn: D. Sachs
Attn: D.G. Hopper

Stanford Research Institute International
Attn: M. Baron
Attn: W.G. Chesnut

Technology International Corporation
Attn: W.P. Boquist

United Technologies Corporation
Attn: R.H. Bullis

Utah State University
Attn: D. Baker
Attn: K. Baker
Attn: C. Wyatt
Attn: A. Steed

DISTRIBUTION LIST (Cont)

Physical Science, Inc.

Attn: K. Wray
Attn: R.L. Taylor
Attn: G. Caledonia

Commander

Rome Air Development Center
Attn: OSCA, J.J. Simons
Attn: OSCA, J.J. Simons

Steward Radiance Laboratory
Attn: R. Huppi

Boston College

Space Data Analysis Laboratory
Attn: E.R. Hegblom
Attn: W.F. Grieder

Forrestial Campus Library
Princeton University
Attn: Librarian

Visidyne, Inc.

Attn: H. Smith
Attn: J.W. Carpenter
Attn: T.C. Degges
Attn: C. Humphrey
Attn: W.P. Reidy

Wayne State University

Attn: R.H. Kummier
Attn: W.E. Kaupplia

END

DATE
FILMED

11-80

DTIC

